6th FERO meeting

Prague, 31 August 2012

Resolving Quasar Accretion Discs by Gravitational Microlensing

David Heyrovský & Lukáš Ledvina

Charles University, Prague

Outline

1. Gravitational lensing principle and properties
2. Quasar microlensing principle and properties
3. UV / optical / X-ray observations of quasar microlensing
4. Microlensing sensitivity to accretion disc parameters

Gravitational lens model

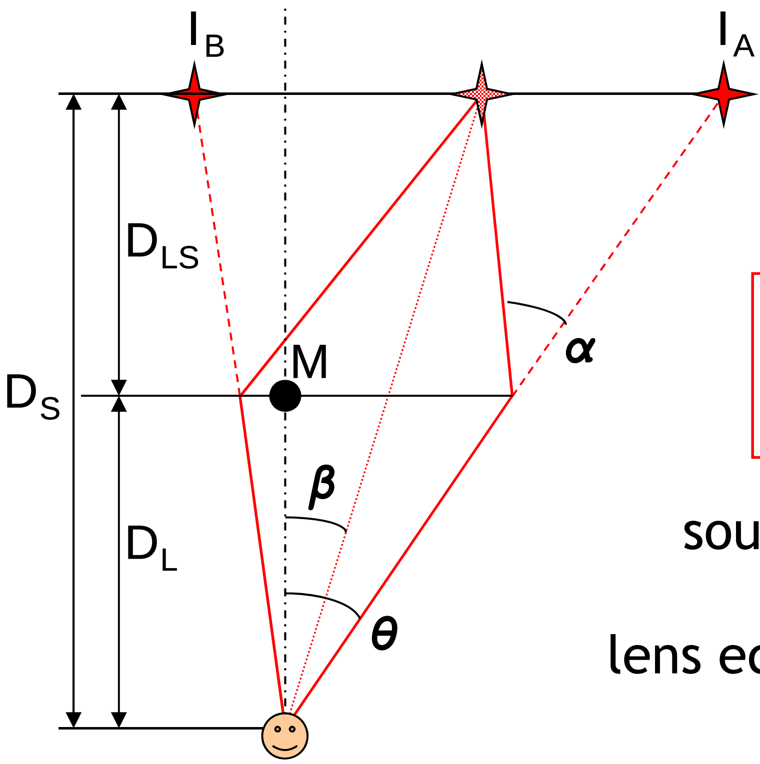

lens equation: $$\boxed{\vec{\beta} = \vec{\theta} - \frac{D_{LS}}{D_S}\vec{\alpha}\left(\vec{\theta}\right)}$$

point-mass lens: $$\vec{\alpha}\,(\vec{\theta}\,) = \frac{4GM}{c^2 D_L \theta^2}\,\vec{\theta}$$

$$\boxed{\theta_E \equiv \sqrt{\frac{4GMD_{LS}}{c^2 D_L D_S}}}$$ Einstein radius

source pos. $\vec{y} \equiv \vec{\beta} / \theta_E$, image pos. $\vec{x} \equiv \vec{\theta} / \theta_E$

lens equation: $$\boxed{\vec{y} = \left(1 - x^{-2}\right)\vec{x}}$$

image positions

$$|\,\vec{y}\,| > 0 \ldots \vec{x}_{A,B} = \left(\frac{1}{2} \pm \sqrt{\frac{1}{4} + y^{-2}}\right)\vec{y}$$

$$|\,\vec{y}\,| = 0 \ldots |\,\vec{x}\,| = 1$$

Images of a point source

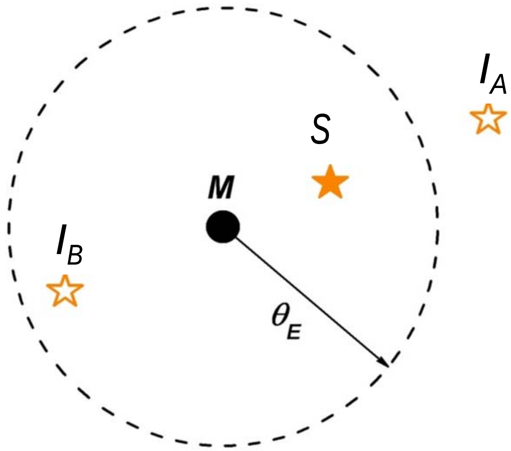

Images of an extended source

each point of the source imaged independently

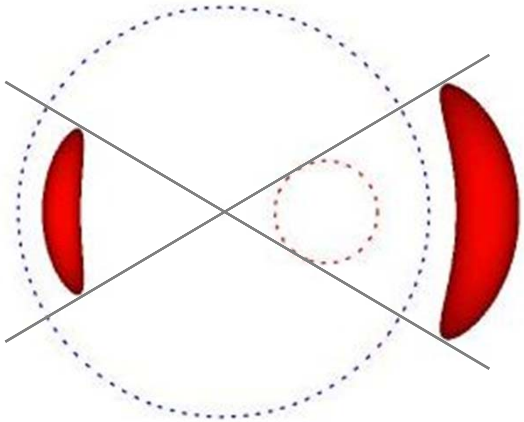

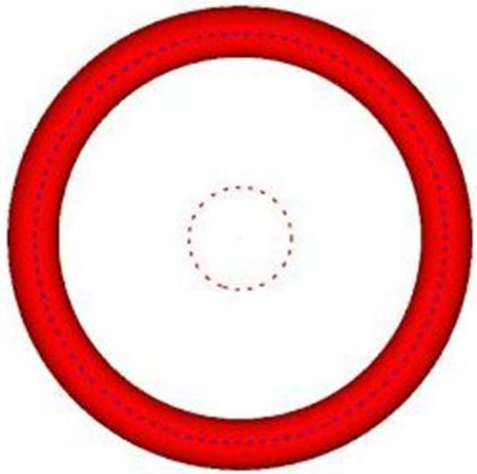

angular magnification of images -> source flux amplification

Quasar 0957+561 (Walsh, Carswell, Weymann 1979)

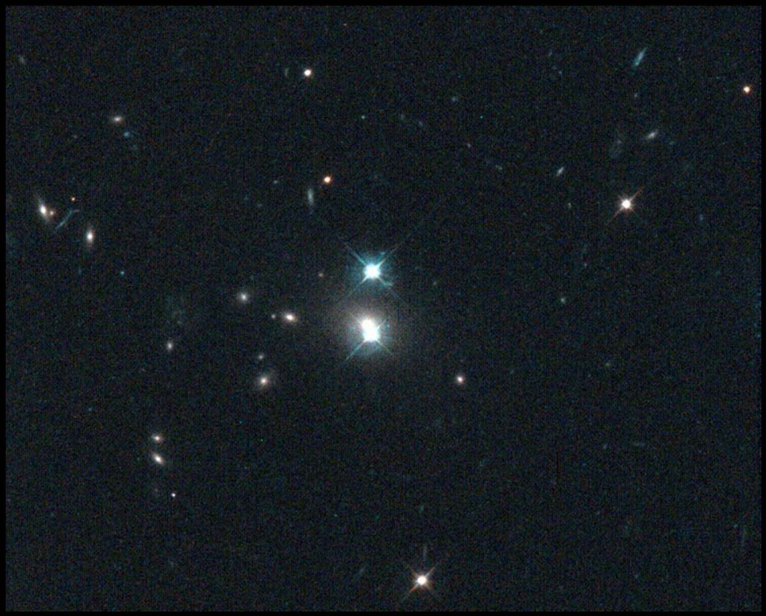

http://www.astr.ua.edu/keel/agn/q0957.html

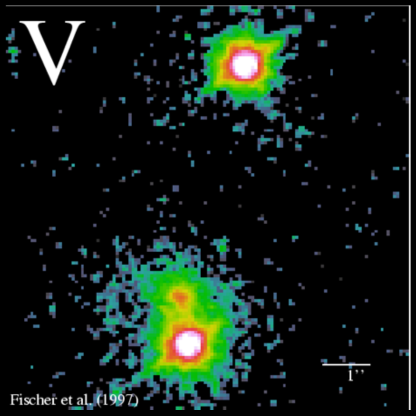

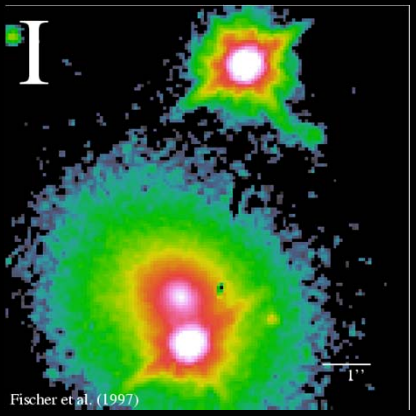

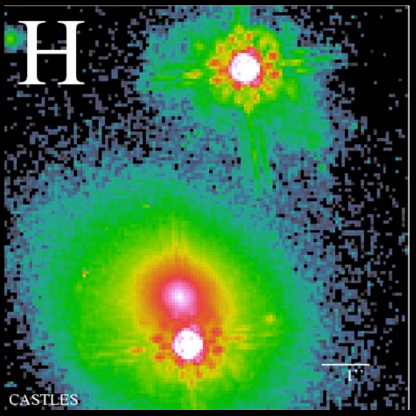

http://cfa-www.harvard.edu/castles/Individual/Q0957.html

Currently known gravitational (macro)lenses

▼ Master Lens Database

Containing 526 Gravitational Lens Systems:

- 328 Grade-A Lenses
- 85 Grade-B Lenses
- 77 Grade-C Lenses

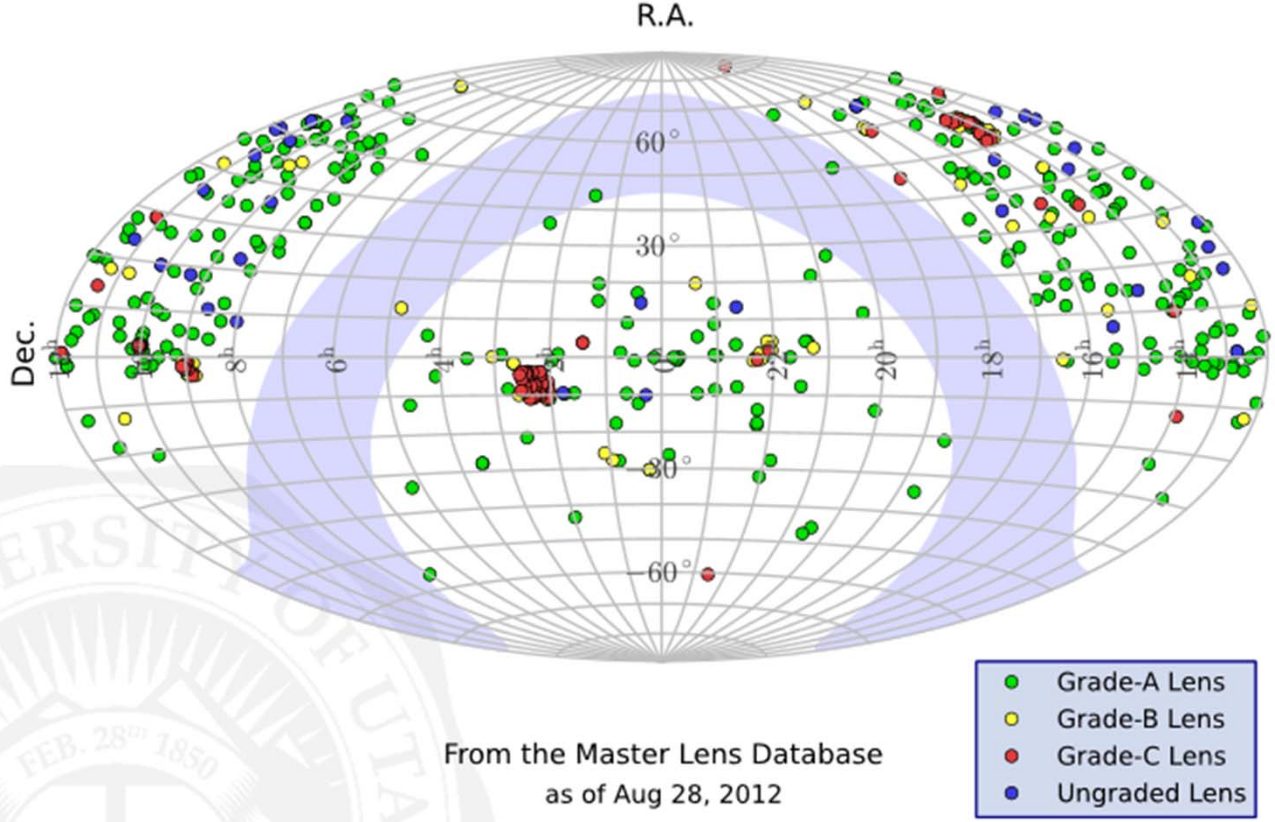

http://masterlens.astro.utah.edu

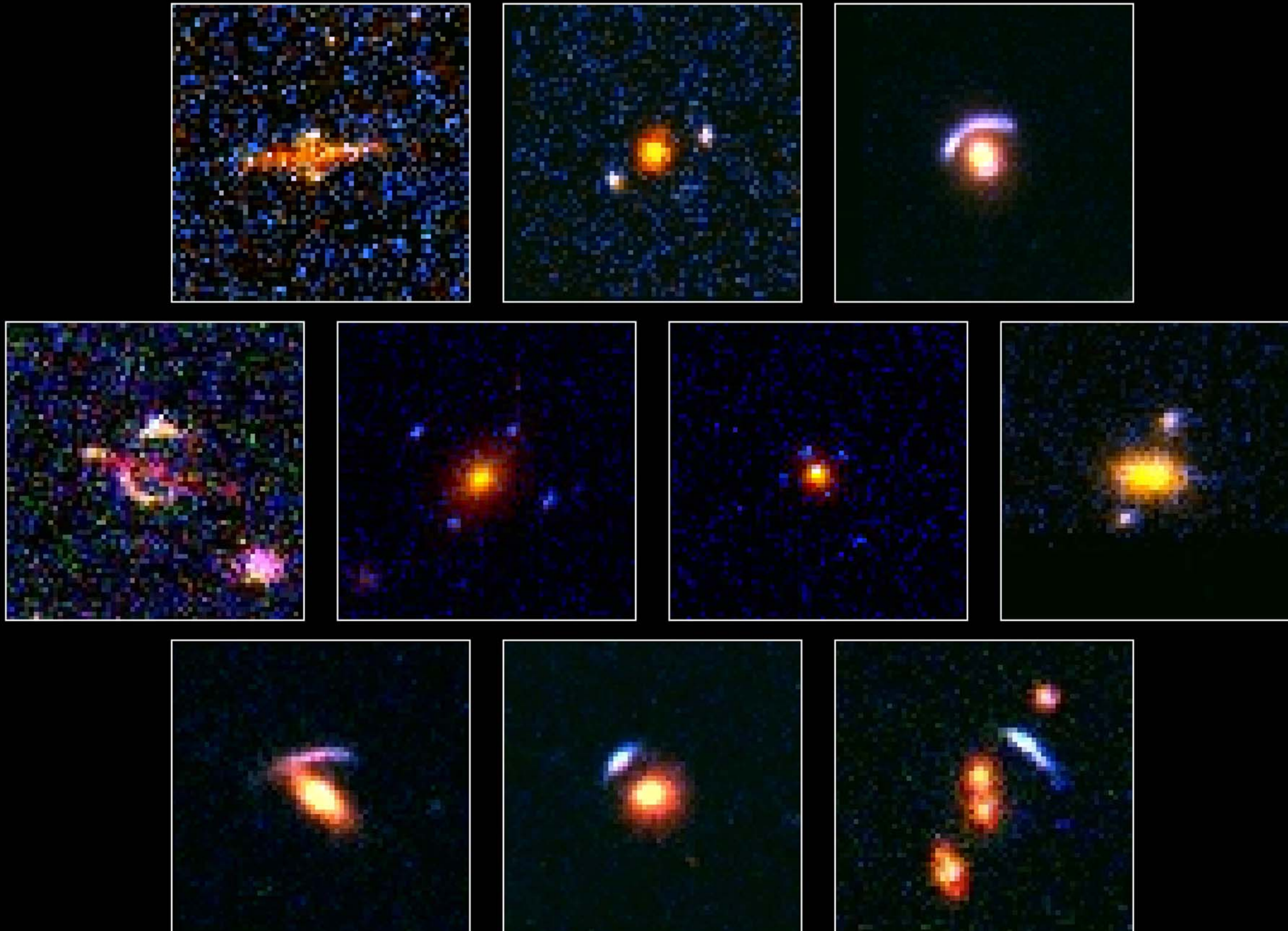

Gallery of Gravitational Lenses

Hubble Space Telescope • WFPC2

PRC99-18 • STScI OPO • K. Ratnatunga (Carnegie Mellon University) and NASA

More realistic gravitational lenses

n point masses:

$$\boxed{\vec{\alpha}(\vec{\theta}) = \frac{4\,G}{c^2 D_L} \sum_{i=1}^{n} M_i \frac{\vec{\theta} - \vec{\theta}_i}{\left|\vec{\theta} - \vec{\theta}_i\right|^2}}$$

continuous mass distribution (surface mass density Σ):

$$\boxed{\vec{\alpha}(\vec{\theta}) = \frac{1}{\pi} \frac{D_S}{D_{LS}} \int \kappa(\vec{\theta}') \frac{\vec{\theta} - \vec{\theta}'}{\left|\vec{\theta} - \vec{\theta}'\right|^2} \mathrm{d}^2\vec{\theta}'} \qquad \kappa(\vec{\theta}') = \frac{\Sigma(D_L \vec{\theta}')}{\Sigma_{CR}} \qquad \Sigma_{CR} = \frac{c^2}{4\pi G} \frac{D_S}{D_L D_{LS}}$$

point-source flux amplification

$$\boxed{A_0(\vec{y}) = \sum_{images} \frac{\mathrm{d}\,\Omega(image)}{\mathrm{d}\,\Omega(source)} = \sum_{images} \left| \frac{\partial\, \vec{y}}{\partial\, \vec{x}} \right|_i^{-1}}$$

$$A_0(\vec{y}) = \infty \quad \text{for source } \vec{y} \in \text{caustic, image } \vec{x} \in \text{critical curve}$$

Imaging by a lens with an ellipsoidal mass distribution

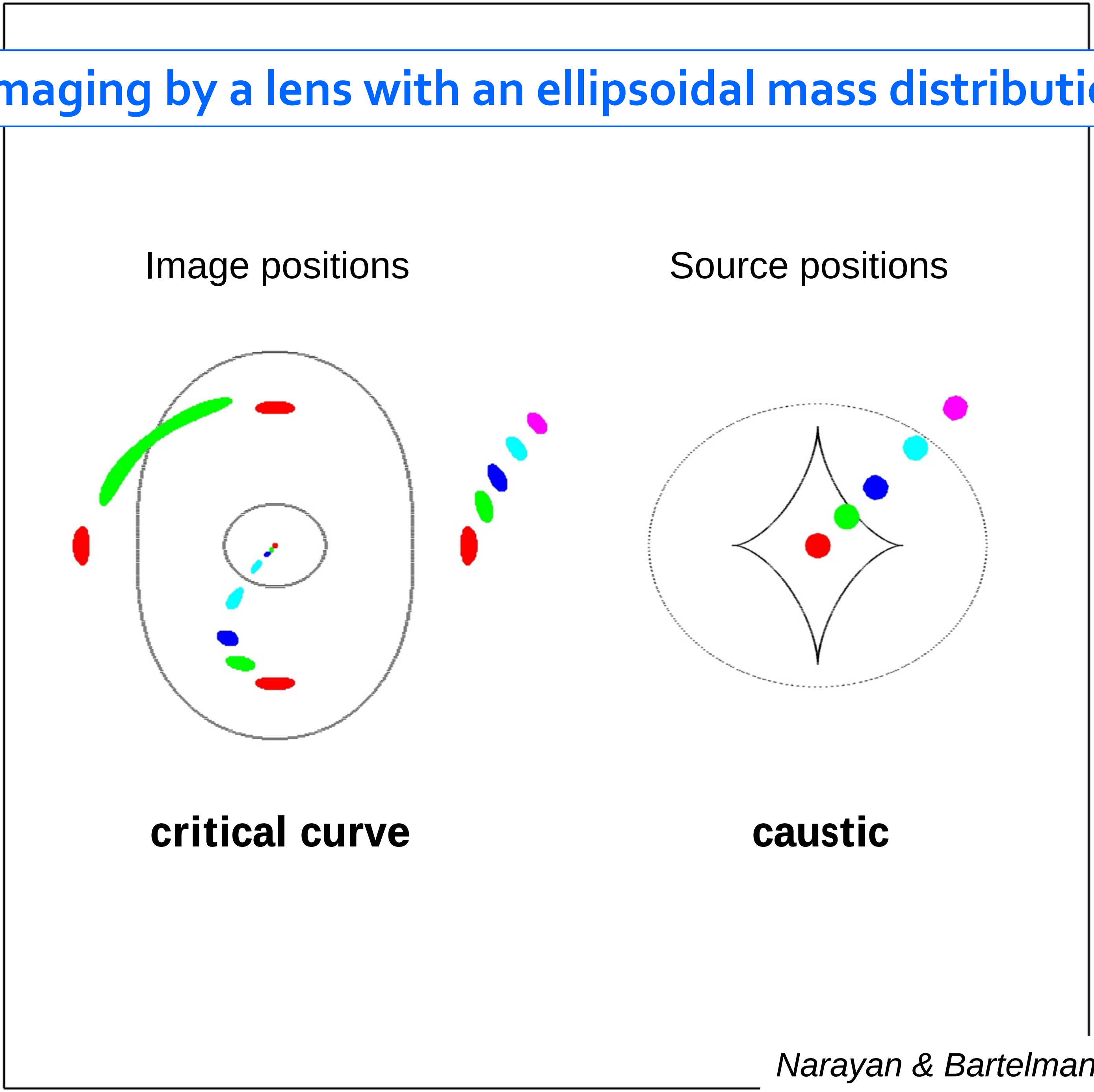

Narayan & Bartelmann (1999)

http://hubblesite.org/newscenter/newsdesk/archive/releases/1990/20/image

Effect of source position and size

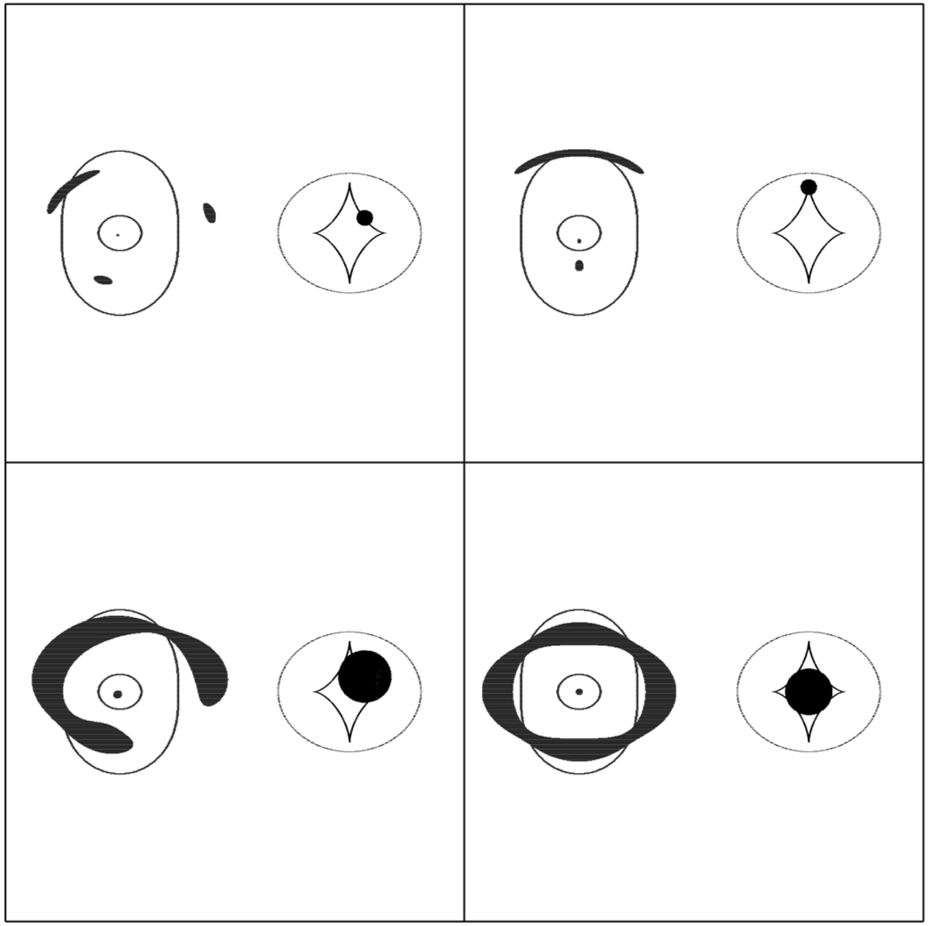

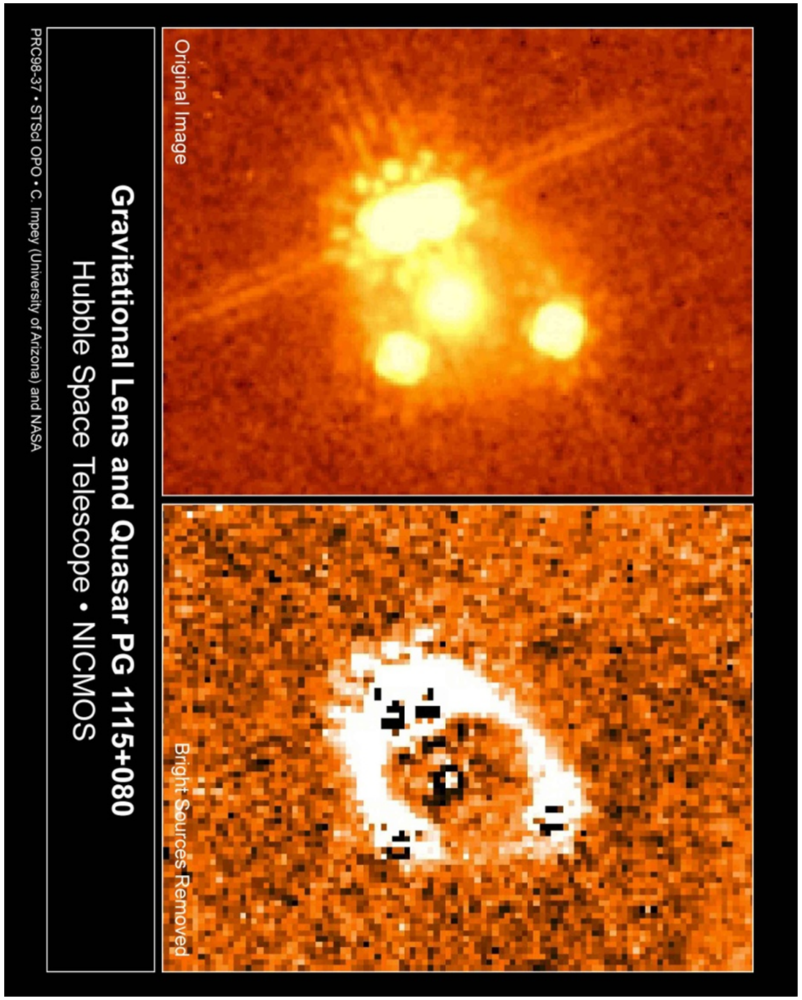

Narayan & Bartelmann (1999)

Quasar microlensing

- angular size of quasar accretion disk comparable to Einstein radii of individual stars in the lens galaxy (micro-arcseconds)
- relative motion of quasar wrt caustic network formed by stars in lens galaxy on timescales of weeks / months

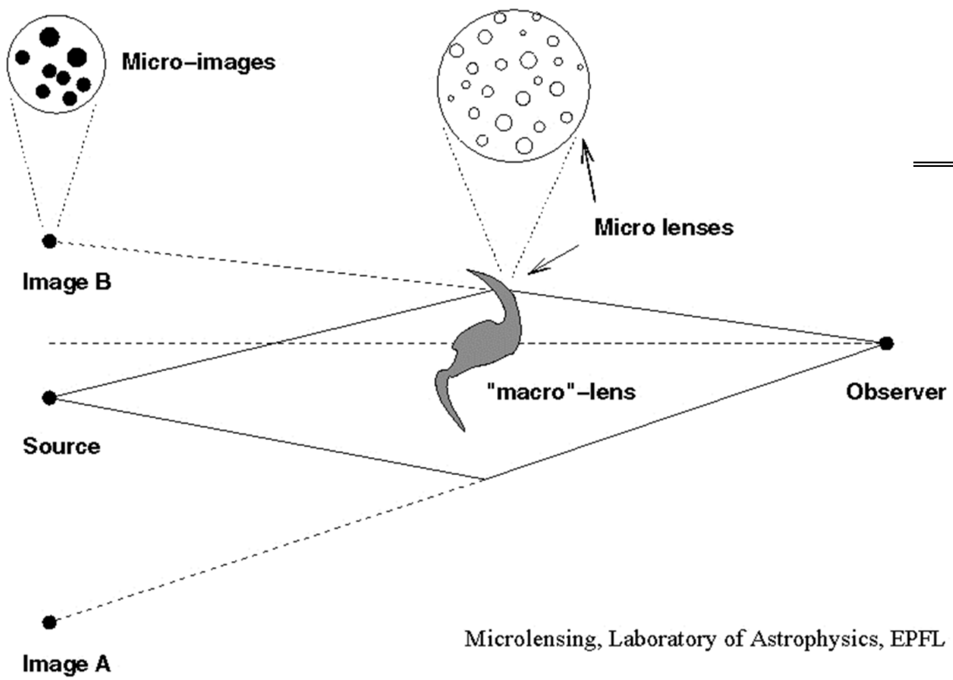

Microlensing, Laboratory of Astrophysics, EPFL

⟶ given image microlensed by the local stellar population

⟶ microimages cannot be resolved, but flux modulation due to microlensing amplification observable

Microlensing vs. intrinsic flux variations

- intrinsic flux variations identical in all macroimages (with time delays)
- microlensing variations are image-specific (don't appear in other images)

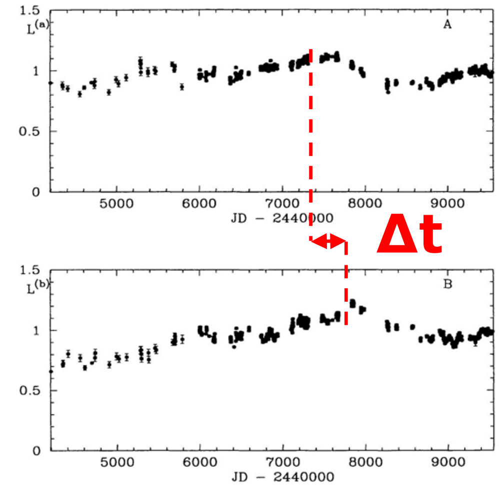

Pijpers (1997)

Microlensing lens equation

$$\vec{y} = \begin{pmatrix} 1-\kappa_c-\gamma & 0 \\ 0 & 1-\kappa_c+\gamma \end{pmatrix} \vec{x} - \sum_i \frac{M_i}{\bar{M}} \frac{\vec{x}-\vec{x}_i}{\left|\vec{x}-\vec{x}_i\right|^2}$$

κ_c, γ depend on lens potential at macroimage position

$M_i, \vec{x}_i$ masses and positions of microlensing stars

$\bar{M}$ average stellar mass

amplification computed numerically using inverse ray shooting

Microlensing amplification map, microimages

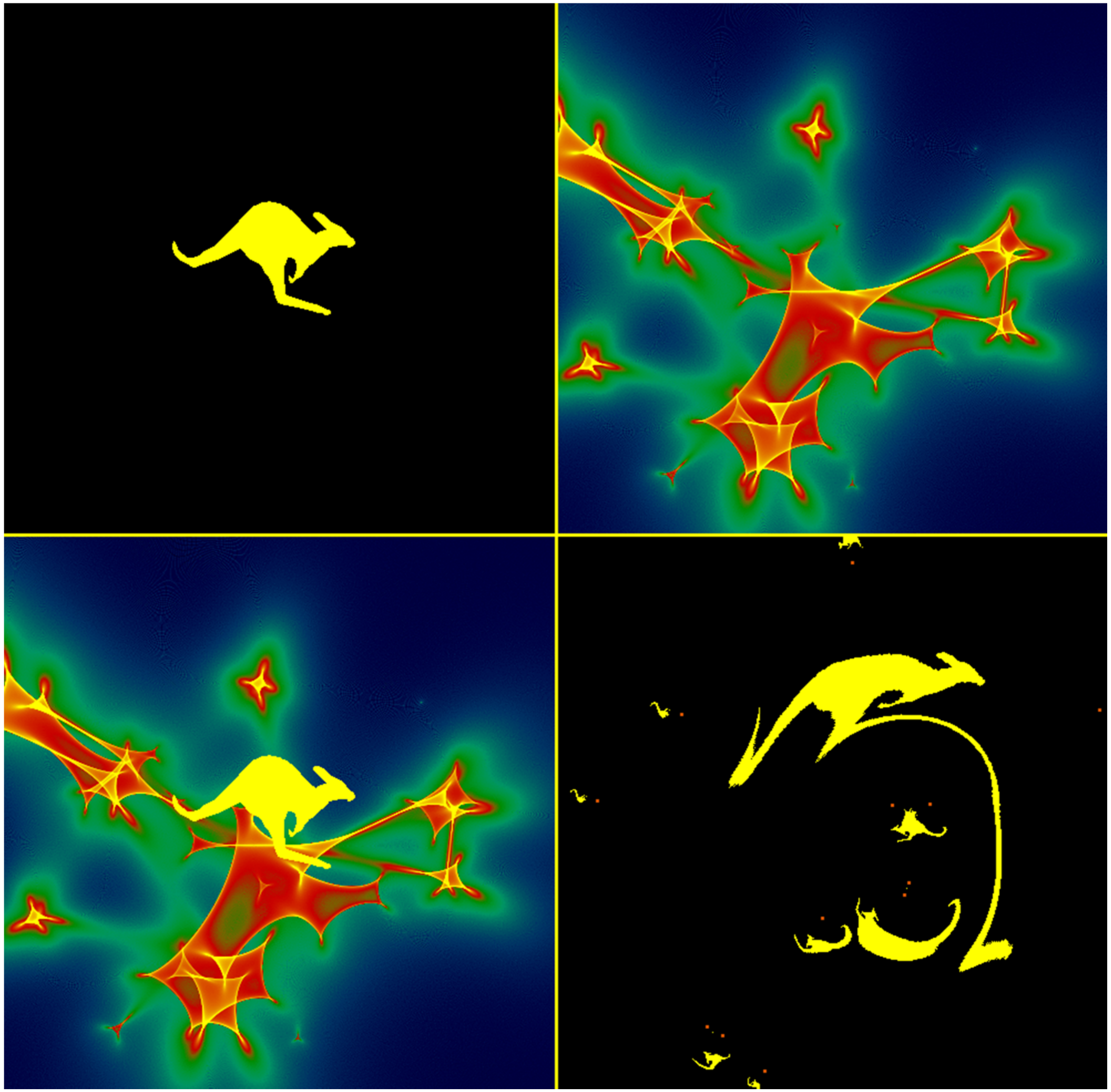

J. Wambsganss

Quasar motion wrt caustic network: light curves

sensitive to quasar structure

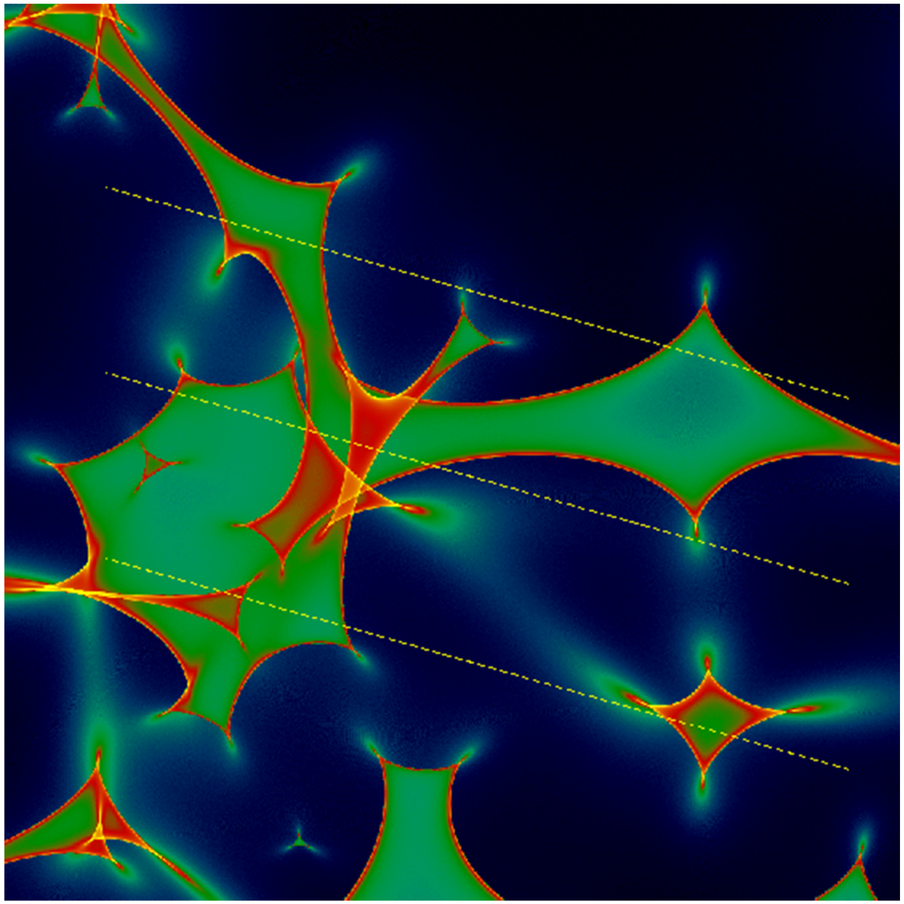

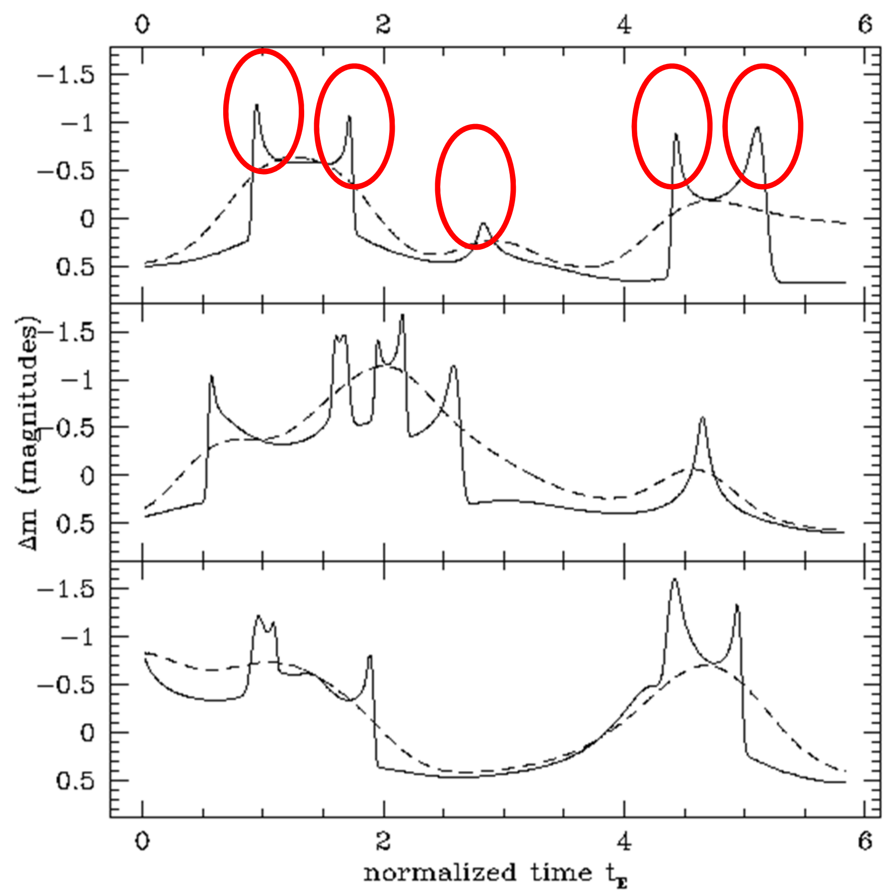

quasar tracks

light curves for Gaussian source widths 0.03 (solid), 0.3 (dashed)

Wambsganss (1998)

Resolving quasar accretion discs by microlensing

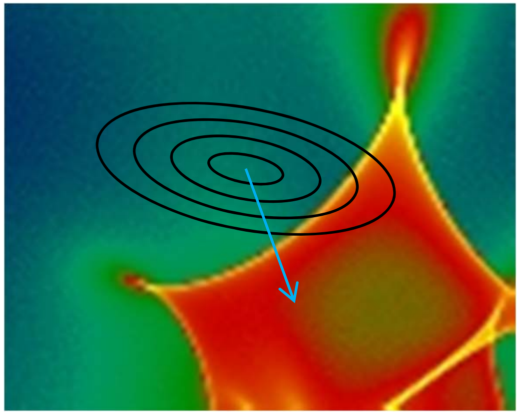

during caustic crossing emission from different parts of disc amplified differently

$\Longrightarrow$ the caustic “scans” the disc surface

Flux from quasar with intensity distribution $I_{obs}(\vec{y}')$ centered at $\vec{y}_c(t)$

$$\boxed{F(\vec{y}_c(t)) = \int_{disc} I_{obs}(\vec{y}')A_0(\vec{y}_c + \vec{y}')\,\mathrm{d}^2\vec{y}'}$$

$\Longrightarrow$ light curve traces the quasar intensity distribution

Advantages of observing in X-rays

- smaller emitting region implies stronger microlensing variation
- only local structure of amplification map important

UV continuum region size in the Einstein Cross QSO 2237+0305 (Eigenbrod et al. 2008)

macroimage A/B flux ratios

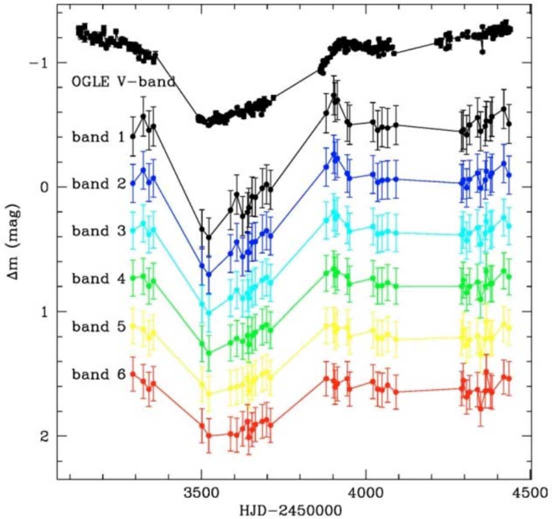

Band	λ_c [Å]	$R_i/R_{\rm ref}$
1	1625	0.73 ± 0.14
2	1875	0.87 ± 0.11
3	2125	1.00 ± 0.09
4	2375	1.13 ± 0.09
5	2625	1.29 ± 0.13
6	2875	1.46 ± 0.18

sample light curves agreeing with data

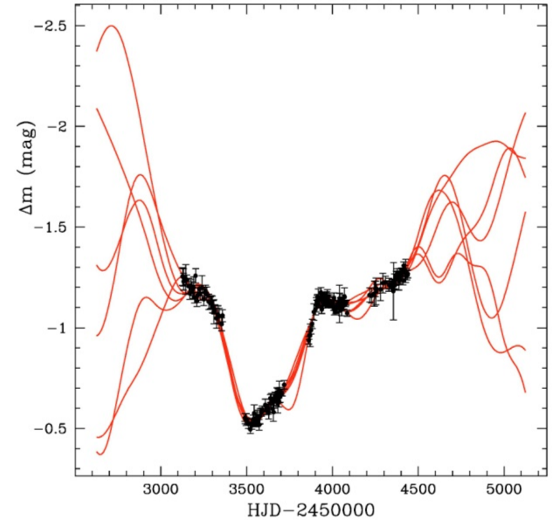

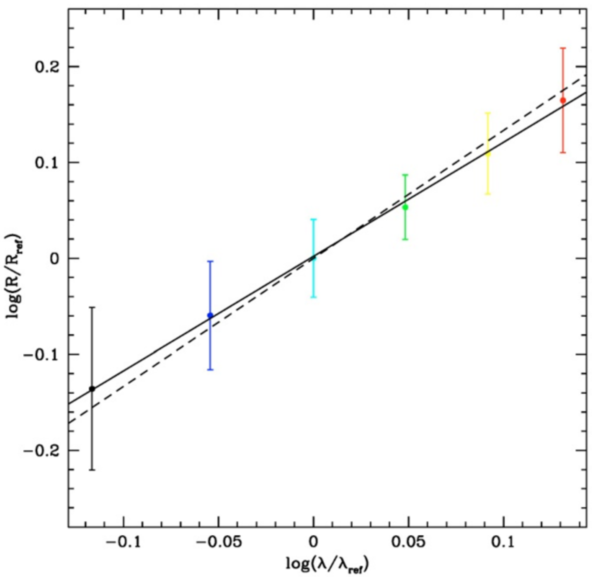

log(size) vs. log(rest wavelength) dependence

$$\boxed{R \propto \lambda^{1.2\pm0.3}}$$

- compatible with thin-disk prediction $R \propto \lambda^{4/3}$

UV / optical continuum region size in 12 quadruply imaged QSOs (Blackburne et al. 2011)

log(size) vs. log(rest wavelength) plots

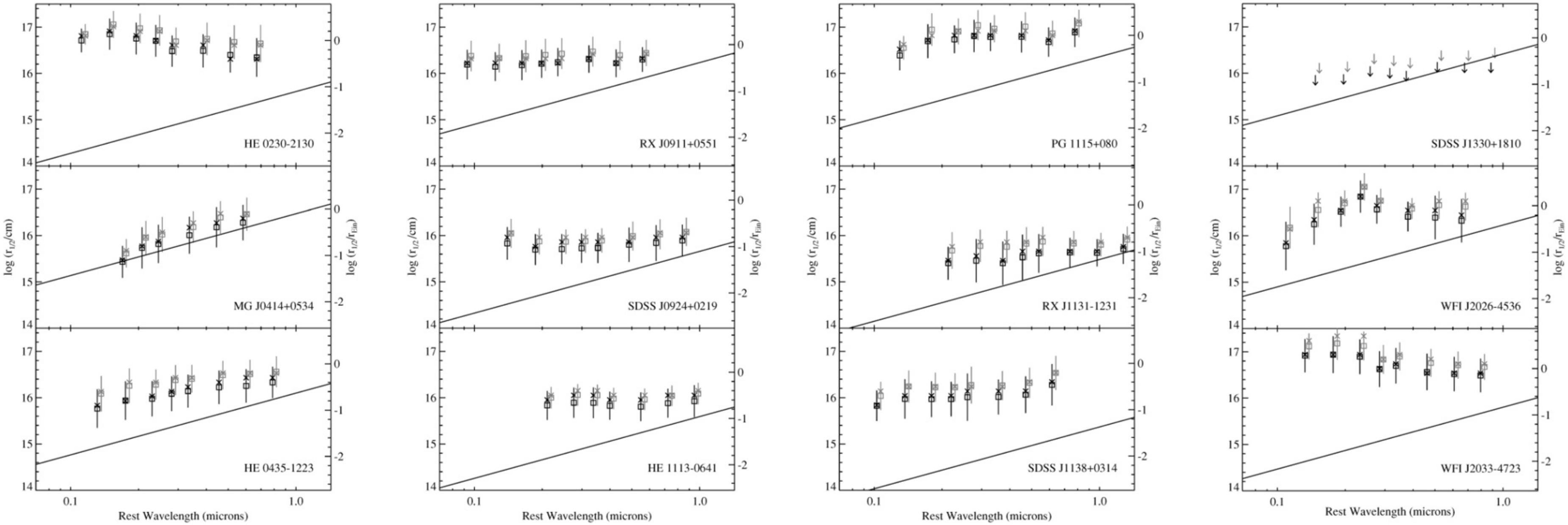

! Only 1 QSO compatible with thin-disk- predicted size and $R \propto \lambda^{4/3}$ scaling !

BLR size in the Einstein cross QSO 2237+0305 (Sluse et al. 2011)

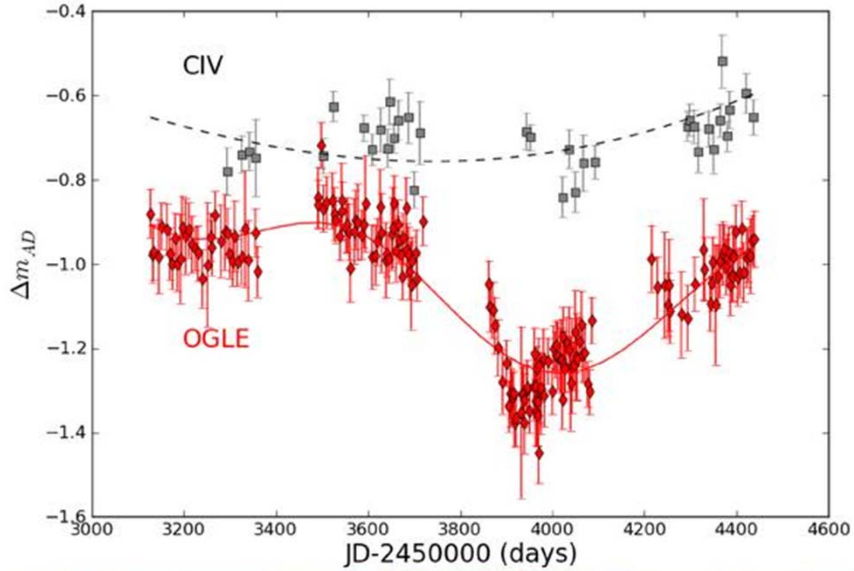

macroimage A/D flux ratio in CIV[1549Å] and in V-band [5500Å] continuum (OGLE)

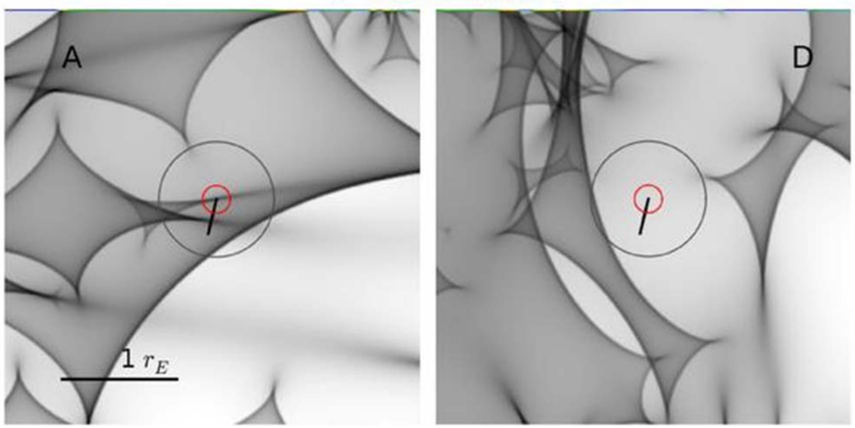

sample A, D amplification maps agreeing with data

$$R_{CIV} = 66^{+110}_{-46} \text{ light-days}$$
$$R_{CIV} / R_{cont} = 4 - 29$$

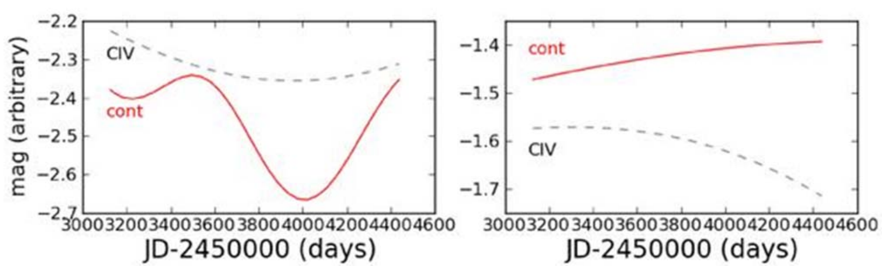

corresponding A, D light curves

X-ray monitoring of gravitational lenses with CHANDRA (Chen et al. 2012)

Lens	z_s [a]	z_l [a]	R.A. (J2000)	Decl. (J2000)	N_H [b] ($\times 10^{22}$ cm^{-2})
QJ 0158−4325	1.29	0.317	01:58:41.44	−43:25:04.20	0.0195
HE 0435−1223	1.689	0.46	04:38:14.9	−12:17:14.4	0.0511
SDSS 0924+0219	1.524	0.39	09:24:55.87	+02:19:24.9	0.0375
SDSS 1004+4112	1.734	0.68	10:04:34.91	+41:12:42.8	0.0111
HE 1104−1805	2.32	0.73	11:06:33.45	−18:21:24.2	0.0462
Q 2237+0305	1.69	0.0395	22:40:30.34	+03:21:28.8	0.0551

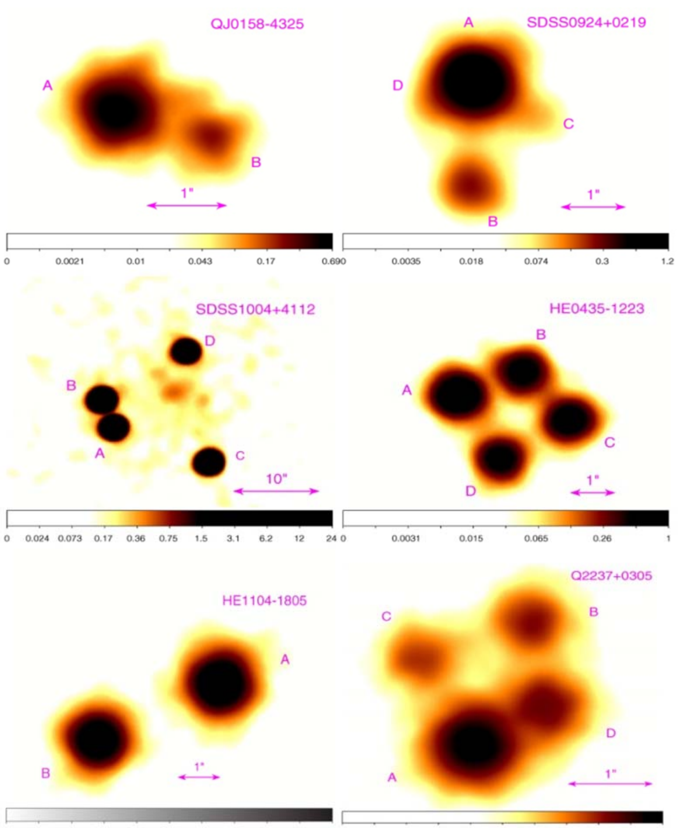

microlensing detected in all 6 systems

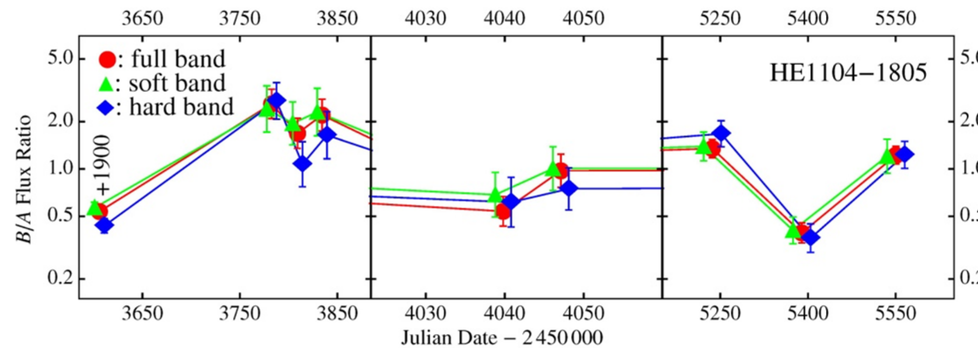

strong Fe Kα line detected in all 6

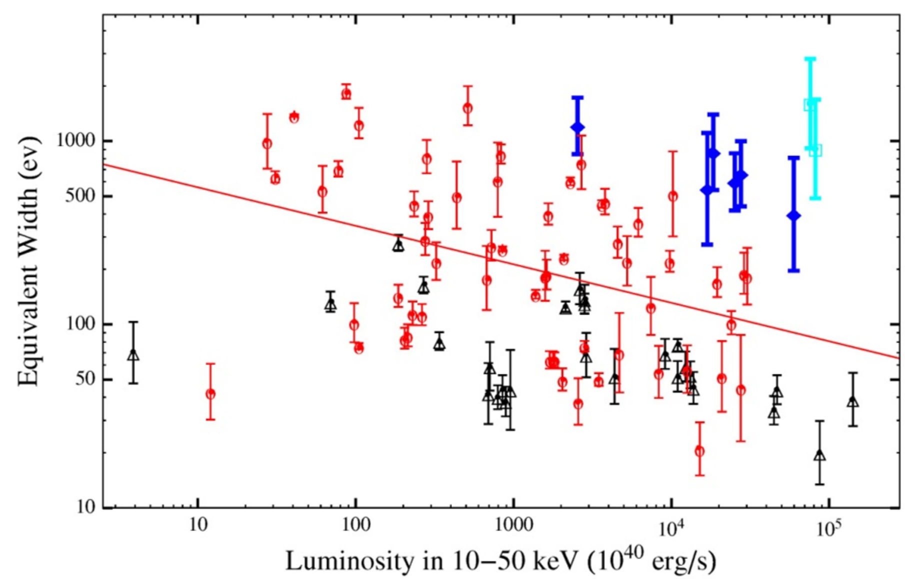

Model of accretion disc (Dovčiak)

- Kerr BH (spin a) + thin disk
- local emission: specific intensity $I_{E,e} \sim E_e^{-\Gamma} r^{-q}$
  - $E_{\rm e}\ldots$ photon energy
  - $r\ldots$ Boyer-Lindquist radius
  - $\Gamma\ldots$ spectral index
  - $q\ldots$ radial index
- observed photon energy $E_{\rm obs} = E_e g$
  g … Doppler + gravitational shift
- transformation $(r, \varphi)_{B-L} \Rightarrow (\alpha, \beta)$ cartesian coordinates of deflected photons
- observed intensity in given energy band:
  $I_{\rm obs}(\alpha, \beta; q, \Gamma) = I_0 g(\alpha, \beta)^{\Gamma+2} r(\alpha, \beta)^{-q}$
- total observed particle flux $F_{\rm obs} = \int_{\rm disk} I_{\rm obs}(\alpha, \beta; q, \Gamma) A_0(\alpha, \beta) {\rm d}\alpha {\rm d}\beta$
  $A_0(\alpha, \beta)$ … microlensing point-source amplification
- disk cutoff at ISCO, at radius including 99% of total flux

Crossing of a microlensing caustic

- local approximation of point-source amplification map by linear fold caustic:

$$A_0(\alpha,\beta) \simeq \begin{cases} 1 & \text{outside caustic} \\ 1 + \sqrt{\frac{d_0}{d_\perp(\alpha,\beta)}} & \text{inside caustic} \end{cases}$$

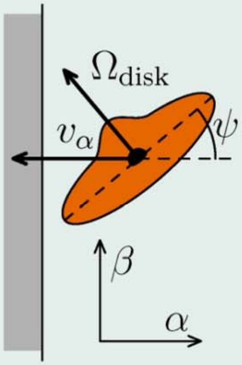

  - $d_\perp(\alpha,\beta)$ . . . perpendicular distance from caustic line
  - d_0 . . . caustic strength, scales light curve peak height

- geometry
  - ψ. . . orientation of disk during caustic crossing

Light curves: dependence on orientation ψ

$q = 3$, $\Gamma = 2$, $i = 60°$ (inclination), $a = 1$

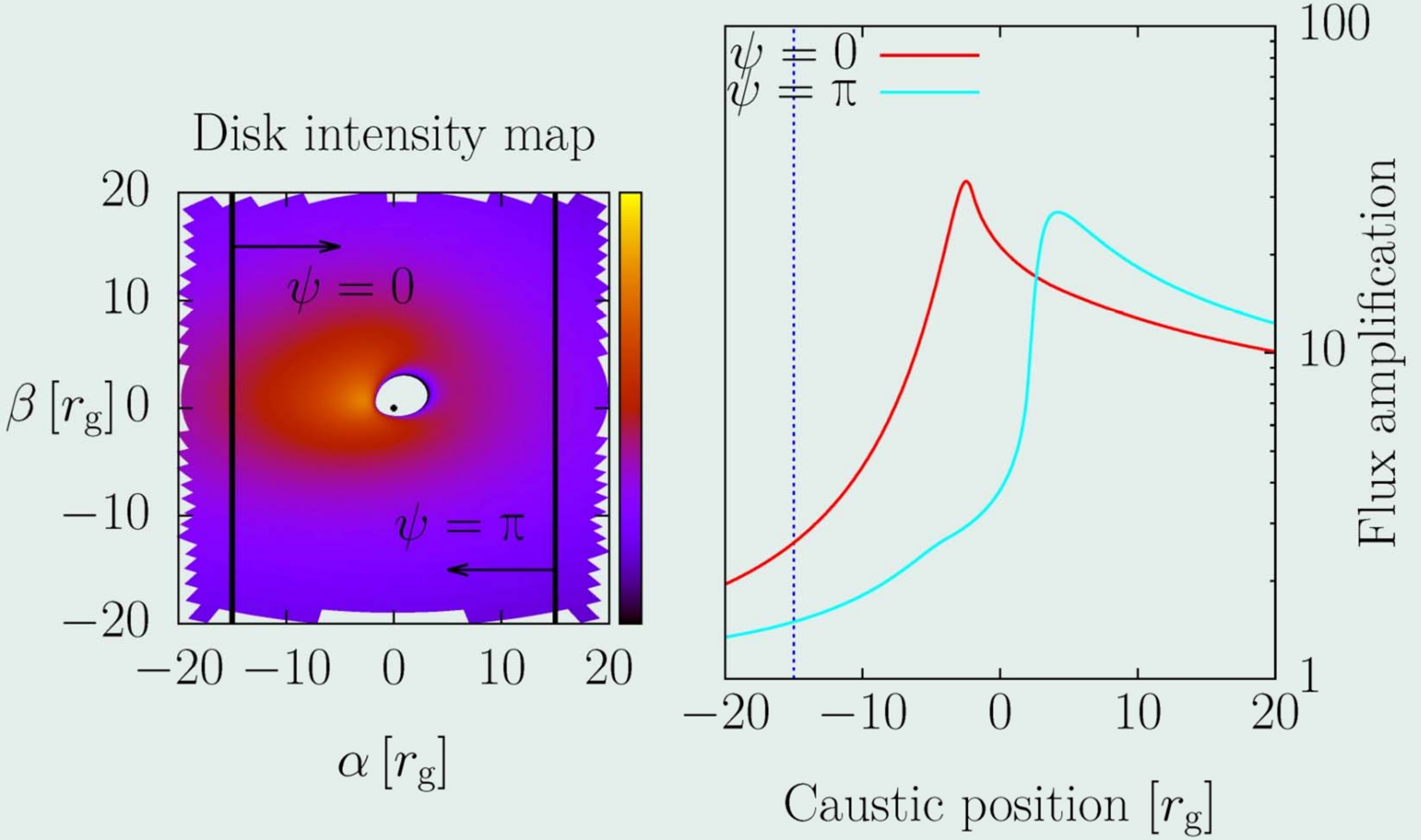

Home Page
Title Page
Contents
Page 4 of 7
Go Back
Full Screen
Close
Quit

Light curves: dependence on spin of BH a

$q = 3$, $\Gamma = 2$, $i = 60°$, $\psi = \pi/4$

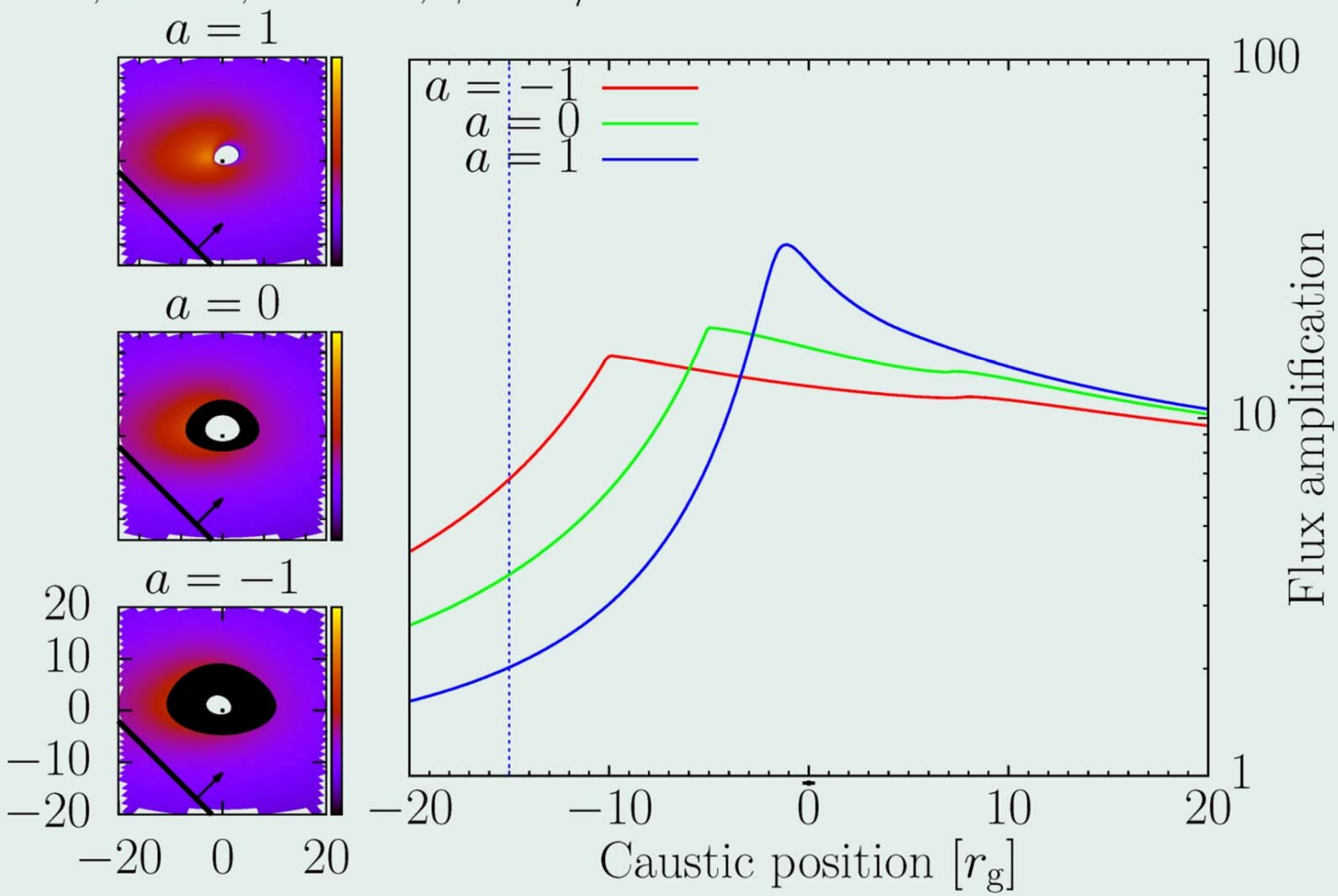

Light curves: dependence on inclination i

$q = 3,\ \Gamma = 2,\ a = 1,\ \psi = \pi/4$

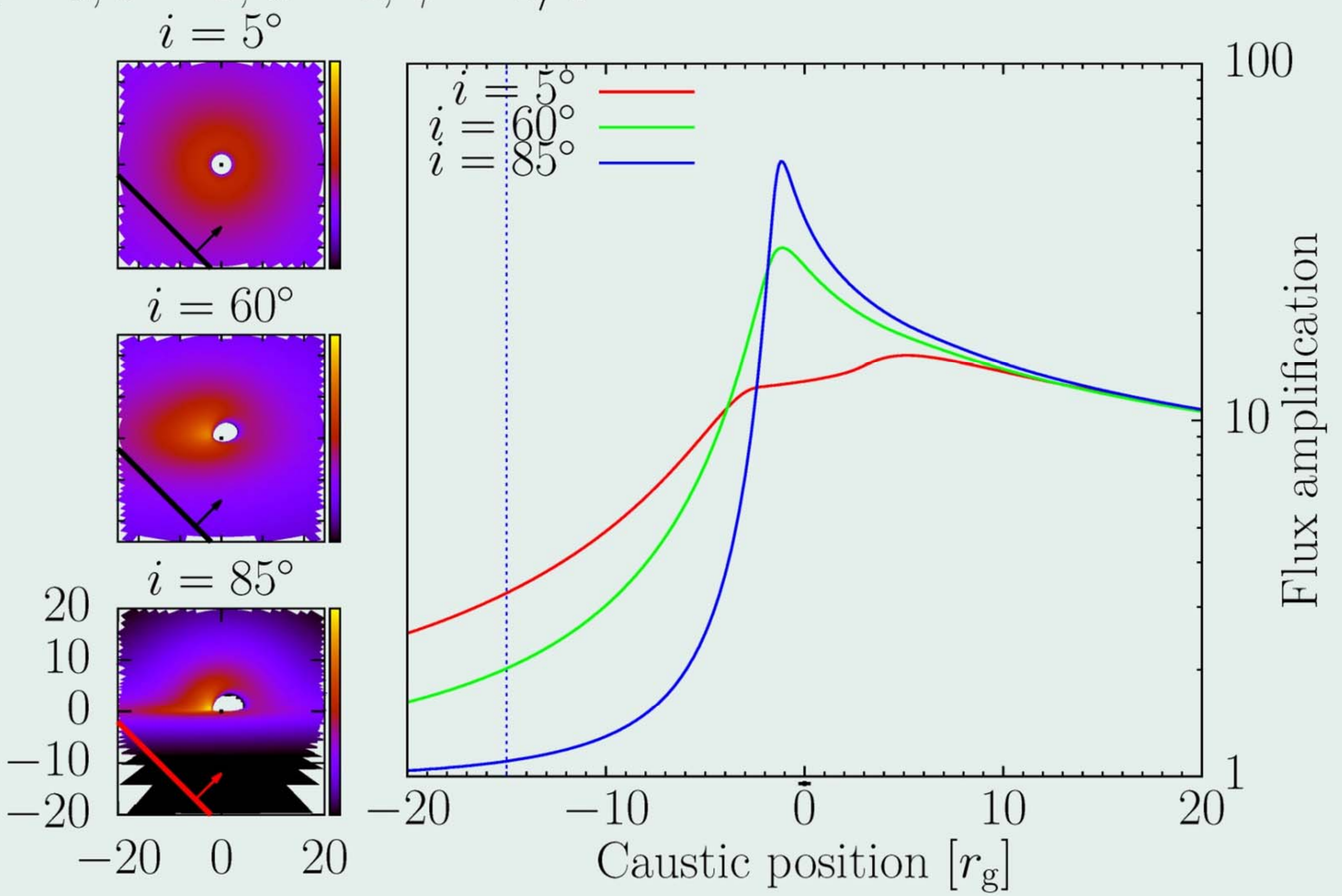

Light curves: dependence on radial index q

$\Gamma = 2,\ i = 60°,\ a = 1,\ \psi = \pi/4$

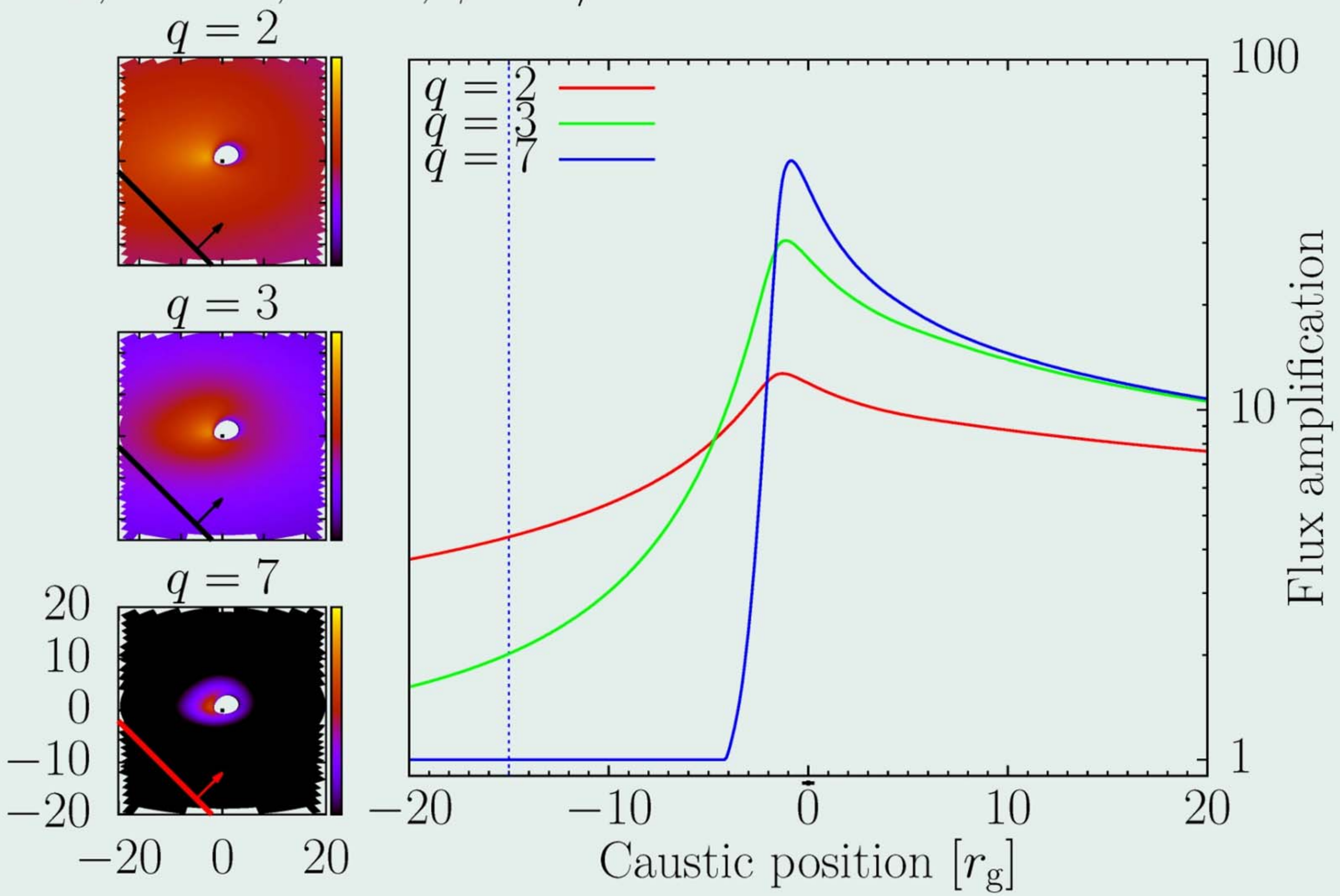

Future

- Use better model of caustic structure or real amplification map
- Study changes of shape of iron K_α line
- Thanks for attention … soon, but not just yet

X-ray microlensing in RX J1131-1231 (Chartas et al. 2012)

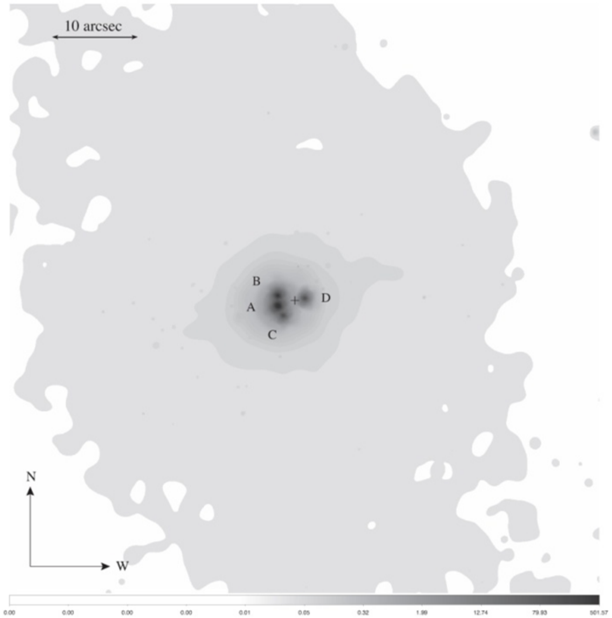

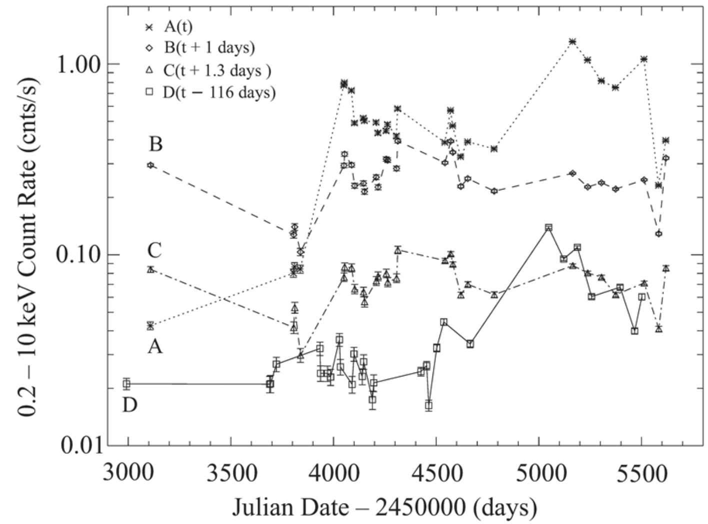

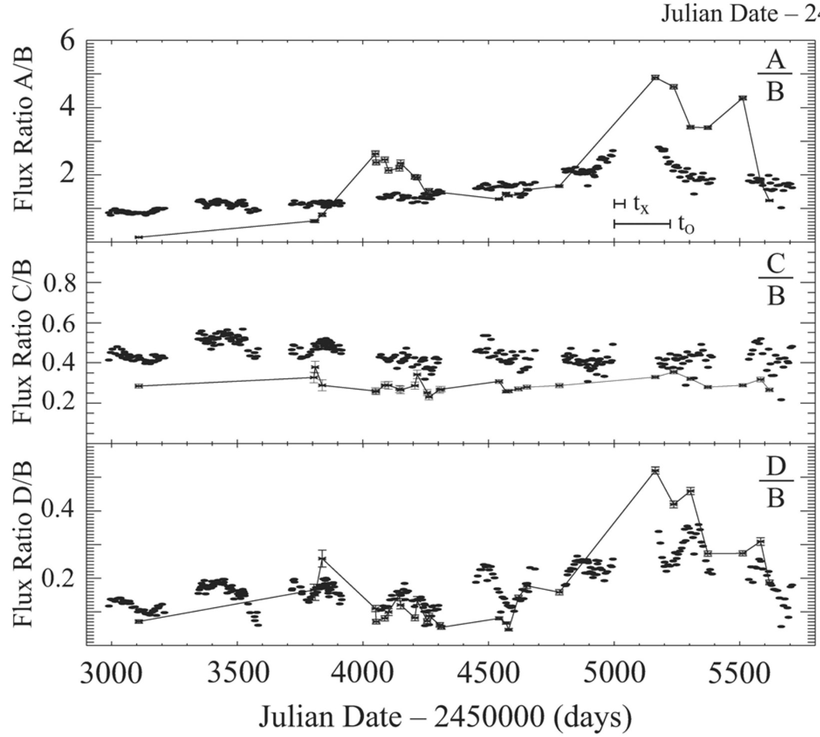

X-ray microlensing in RX J1131-1231 (Chartas et al. 2012) – cont'd

Fe Kα changes during caustic crossing !